Applied Catalysis B: Environmental 156–157 (2014) 323–330

Contents lists available at ScienceDirect

Applied Catalysis B: Environmental

journal homepage: www.elsevier.com/locate/apcatb

An efficient visible-light photocatalyst prepared from g-C_3N_4 and polyvinyl chloride

Desong Wang*, Haitao Sun, Qingzhi Luo, Xiaolian Yang, Rong Yin

School of Sciences, Hebei University of Science and Technology, Shijiazhuang 050018, People's Republic of China

ARTICLE INFO

Article history:
Received 2 January 2014
Received in revised form 17 March 2014
Accepted 19 March 2014
Available online 28 March 2014

Keywords:
Photocatalyst
Visible light photocatalytic activity
g-C_3N_4
Conjugated polymer
Polyvinyl chloride

ABSTRACT

A facile method has been developed to prepare an efficient visible-light photocatalyst using g-C_3N_4 and ordinary polyvinyl chloride (PVC) as main precursors. Firstly, g-C_3N_4 was dispersed into PVC solution with tetrahydrofuran as solvent. Secondly, the above suspension containing g-C_3N_4 was heated at 50 °C to obtain PVC/g-C_3N_4 composite via solvent volatilization. Finally, the product was heated at 150 °C for 2 h to obtain the photocatalyst covered by a small amount of conjugated polymer derived from PVC via dehydrochlorination reaction. The as-prepared photocatalyst was characterized by Scanning electron microscopy, UV–vis diffuse reflectance spectroscopy, X-ray diffraction, X-ray photoelectron spectroscopy, Raman Spectroscopy, photoluminescence spectroscopy, etc. The photocatalytic activity of the as-prepared photocatalyst was evaluated by photodegradation of Rhodamine B solution under visible-light irradiation. The results show that the conjugated polymer can obviously improve the absorbance of g-C_3N_4 in the visible light range and the BET specific surface area, and hardly affect its crystalline structure. The visible-light photocatalytic activity of the as-prepared photocatalyt is much higher than that of pure g-C_3N_4, and increases first and then decreases as the content of conjugated polymer on the photocatalyst surface increases. The visible-light photocatalytic mechanism has been discussed.
© 2014 Elsevier B.V. All rights reserved.

1. Introduction

The semiconductors as photocatalysts have been widely investigated for degradation of organic contaminants in water or air and for water-splitting to prepare hydrogen and oxygen [1–3]. Among these semiconductors, TiO_2 is most systematically and deeply investigated due to its high chemical stability, high photocatalytic activity, nontoxicity, low cost, and reusability [4–6]. However, the wide band gap of anatase TiO_2 (3.2 eV) limits its practical utilization in a large scale under solar or in-door light irradiation. Consequently, many approaches have been devoted to overcome the above-mentioned drawback, such as noble metal depositing [7], metal ion or nonmetal atom doping [8,9], dye photosensitizing [10], narrow band gap semiconductor coupling [11], and conjugated-polymer modification [12]. Additionally, the other types of visible-light photocatalysts have been designed and investigated, e.g., sulfides [13], Ag_3PO_4 [14], AgX(X = Cl, Br and I) [15], etc.

Recently, Wang et al. first reported polymeric graphitic carbon nitride (g-C_3N_4) as a promising "metal-free" visible-light photocatalyst for photocatalytic evolution of H_2 and O_2 via water-splitting and for photodegradation of organic pollutants [16]. In general, g-C_3N_4, which is composed of carbon, nitrogen and a small amount of hydrogen, can be synthesized by a facile method such as direct calcination of melamine, urea or cyanamide [17–19]. Additionally, g-C_3N_4 is highly stable with respect to chemical, thermal, and light irradiation due to the strong covalent bonds between carbon and nitride atom. Therefore, g-C_3N_4 is thought to be an important visible-light photocatalyst for practical application in a large scale, and has been drawn intense attentions for many researchers [20–26].

Unfortunately, g-C_3N_4 has two main drawbacks as an efficient visible-light photocatalyst. Firstly, the separation efficiency of photogenerated electron–hole pairs in g-C_3N_4 material is low, indicating its lower visible-light photocatalytic efficiency. Secondly, the band gap of g-C_3N_4 (2.7 eV) allows it to be excited only by the light with the wavelength less than ca. 450 nm, resulting in its inefficient utilization of the light with the wavelength more than 450 nm. To solve the above-mentioned problems and prepare an efficient visible-light g-C_3N_4-based photocatalyst, some methods have been developed, e.g., synthesizing mesoporous structure [27], doping with metal or nonmetal elements [28–30], coupling with other semiconductors [31], and modifying by conjugated polymers [32]. Among these

* Corresponding author. Tel.: +86 311 81669901; fax: +86 311 81669901.
E-mail addresses: dswang06@126.com, wangdesong@hebust.edu.cn (D. Wang).

http://dx.doi.org/10.1016/j.apcatb.2014.03.034
0926-3373/© 2014 Elsevier B.V. All rights reserved.

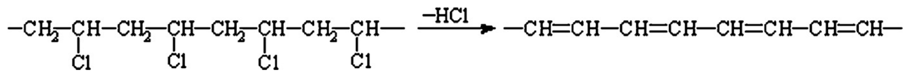

Scheme 1. Main reaction to prepare the conjugated polymer from PVC.

strategies, the conjugated polymer modification has attracted many attentions of the scientists because the conjugated polymers possess high absorption coefficients in the visible spectrum from 400 to 800 nm and good hole conductivity. Ge et al. reported that a novel polyaniline–graphitic carbon nitride (PANI/g-C_3N_4) composite photocatalyst was synthesized by "*in situ*" deposition oxidative polymerization of aniline in the presence of g-C_3N_4 powder in an ice bath [32]. They found that the novel photocatalyst exhibited significantly enhanced visible-light photocatalytic acitivity.

Polyvinyl chloride (PVC) is one of the most common polymers and widely used in many application fields such as building materials, films, and coatings. When PVC is heated at high temperatures such as 150 °C, the dehydrochlorination reaction will easily occur (Scheme 1), and a new polymer with partially conjugated polymer (CPVC) can be produced through elimination of HCl molecules from PVC molecules [33–36]. Consequently, it is reasonable to infer that the visible-light photocatalytic activity of g-C_3N_4 can be greatly improved by the modification of the conjugated polymer derived from ordinary PVC.

In this paper, a facile method has been developed for preparation of "metal-free" photocatalyst (CPVC/g-C_3N_4) with g-C_3N_4 as matrix and a small amount of the conjugated polymer derived from PVC as modifying agent. The as-prepared CPVC/g-C_3N_4 photocatalysts were characterized by Scanning electron microscopy (SEM), UV–vis diffuse reflectance spectroscopy (UV–vis DRS), X-ray diffraction (XRD), X-ray photoelectron spectroscopy (XPS), Raman Spectroscopy, photoluminescence spectroscopy (PL), etc. The visible-light photocatalytic activity and stability was investigated by evaluating the photodegradation of Rhodamine B (RhB).

2. Experimental

2.1. Materials

Melamine, tetrahydrofuran, ethanol and methanol were purchased from Beijing Chemical Reagents Company, China. All the reagents were of AR grade and used without further purification. PVC (R-1069, Tianjin Botian Chemical Co., Tianjin, China) was purified by reprecipitation from tetrahydrofuran solution into methanol for 2 times. The precipitate was dried at room temperature under reduced pressure for more than 2 days. TiO_2 (P25) was purchased from Degussa Corporation, Germany. Deionized water was used in all the experiments.

2.2. Synthesis of CPVC/g-C3N4 photocatalysts

The g-C_3N_4 sample was prepared by directly heating melamine in a semiclosed system according to the literature [16]. In a typical synthesis, 10 g of melamine was firstly heated in a muffle furnace from room temperature to 520 °C with a heating rate of 4 °C min^{-1}. After calcination at 520 °C for 2 h, the as-prepared g-C_3N_4 was cooled naturally to room temperature, and then was grinded for further use.

The CPVC/g-C_3N_4 composite photocatalysts were prepared according to the following steps. Firstly, a small amount of purified PVC was dissolved in 10 mL of tetrahydrofuran. Secondly, 1.0 g of g-C_3N_4 was added into the above-mentioned PVC solutions with different mass ratios of PVC and g-C_3N_4 (1:50, 1:100, 1:200, 1:300, and 1:400), and was magnetically stirred for 2 h. Thirdly, these suspensions were heated at 50 °C to obtain PVC/g-C_3N_4 composites via solvent volatilization. Finally, the products were dried under reduced pressure until the constant mass was reached, and then were heated at 150 °C for 2 h to obtain CPVC/g-C_3N_4 composite photocatalysts. The resultant samples were labeled as CPVC/g-C_3N_4 (1:x), where 1:x is the mass ratio of PVC and g-C_3N_4 in the above-mentioned suspensions for preparation of CPVC/g-C_3N_4 photocatalysts. Scheme 2 describes the preparation procedure of CPVC/g-C_3N_4 photocatalysts.

2.3. Characterization

The morphology of the samples was examined by field emission scanning electron microscopy (SEM, HITACHI S-4800-I) with an accelerating voltage of 10 kV. The X-ray diffraction (XRD) patterns of the CPVC/g-C_3N_4 composite and pure g-C_3N_4 were determined in the range of $2\theta = 10–90°$ by step scanning on a Rigaku D/MAX-2500 diffractometer (Rigaku Co., Japan) with Cu Ka radiation ($k = 0.15406$ nm) as X-ray source, operated at 40 kV and 100 mA. UV–vis diffuse reflectance spectroscopy (UV–vis DRS) was performed in the range of 200–800 nm with $BaSO_4$ as the background on a SHIMADZU-2550 Scan UV–vis system equipped with an integrating sphere attachment (Shimadzu Co., Japan). Raman spectroscopy was performed by a Nicolet 6700 Raman microspectrometer at a resolution of 2 cm^{-1} using the 514.5 nm line of an Ar ion laser as the excitation. The accelerating voltage of 30 kV and emission current of 30 mA were used. X-ray photoelectron spectroscopy (XPS) measurements were recorded on a PHI 5000C ESCA system with Al Ka radiation ($h\nu = 1486.6$ eV). The X-ray anode was run at 250 W and the high voltage was kept at 15.0 kV with a detection angle of 54°. The Brunauer–Emmett–Teller

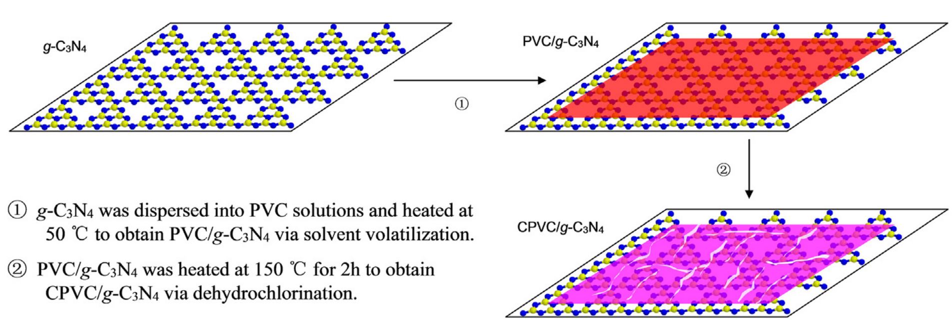

Scheme 2. Idealized formation model of CPVC/g-C_3N_4 photocatalyst.

(BET) surface area measurements of the investigated samples were performed by a Micromeritics NOVA 2000 (Quantachrome, America) surface area analyzer at 77 K using nitrogen as adsorption gas. The photoluminescence (PL) emission spectra of samples were detected with a Fluorescence spectrophotometer (F-4600 FL Spectrophotometer, Hitachi, Japan) using a Xenon lamp as the excitation source at room temperature. The excitation wavelength was 316 nm. Cyclic voltammetry measurements were carried out using an electrochemical system (CHI660D, China). CPVC was deposited as a film on a 1.0 cm × 0.5 cm indium–tin–oxide conducting glass to obtain the working electrode. Ag/AgCl and Pt were employed as the reference electrode and counter electrode, respectively. Supporting electrolyte was 0.1 M $(NH_4)_2SO_4$ solution. Electrochemical impedance spectra (EIS) were performed on an electrochemical system (Solartron 1255B frequency response analyzer and Solartron SI 1287 electrochemical interface) with 0.1 M KCl solution as the electrolyte and FTO/CPVC/*g*-C_3N_4 or FTO/*g*-C_3N_4 electrode as the working electrode. CPVC/*g*-C_3N_4 and *g*-C_3N_4 films were coated on the FTO substrates (fluorine-doped SnO_2, 15 Ω/sq) using a doctor-blade method. The counter and reference electrodes were platinum and saturated calomel electrode (SCE), respectively.

2.4. Photocatalytic activity measurement

The photodegradation of RhB was used to evaluate the visible-light photocatalytic activities of the CPVC/*g*-C_3N_4 composites, the reference samples (*g*-C_3N_4 and commercial TiO_2 P25). Aqueous RhB solution (100 mL) with an initial concentration of 4 mg L^{-1} was placed into a cylindrical glass vessel. Then, the CPVC/*g*-C_3N_4 composites or pure *g*-C_3N_4 (0.10 g) were added into the glass vessel under continuous stirring. Before irradiation, the suspensions were continuously stirred for 1 h in the dark in order to reach an adsorption–desorption equilibrium. After that, the system was irradiated by the visible light emitted from a 300 W iodine tungsten lamp (Philips Co.) with a 400 nm optical filter. The distance between the surface of the suspension and the light source was about 30 cm. The glass reactor was open to ensure the entry of enough oxygen into the system. During irradiation, the samples were taken out every 20 min from the reactor. The photocatalysts were separated from the mixture solution by high-speed centrifugation. The clarified solution was analyzed by a 723 UV–vis spectrometer (Shanghai Spectrum Instruments Co., Ltd., China), and the absorbance of RhB was measured at a wavelength of 552 nm, corresponding to the maximum absorbance wavelength of RhB solution at natural pH conditions. The concentration of RhB solution was obtained by a calibration curve. The symbols of c_0 and c are the concentrations of RhB before and after photoirradiation, respectively.

3. Results and discussion

3.1. Characterization of CPVC/g-C_3N_4 composites

Fig. 1 illustrates the XRD patterns of CPVC/*g*-C_3N_4 (1:300) and pure g-C_3N_4. The pure g-C_3N_4 has two distinct diffraction peaks at 27.7° and 13.1°, which can be indexed to the hexagonal phase of graphitic C_3N_4 (JCPDS 87-1526). The peak at 27.7° as the (0 0 2) plane of *g*-C_3N_4 is due to the interlayer stacking of the conjugated aromatic system, while the peak at 13.1° as the (1 0 0) plane of *g*-C_3N_4 is associated with an in-plane structural packing motif. These two diffraction peaks are in good agreement with the results reported in the literature [37]. Compared with the XRD pattern of pure *g*-C_3N_4, there is no new diffraction peaks in the XRD pattern of CPVC/*g*-C_3N_4 (1:300), indicating that CPVC on the composite surface does not change the crystal structure of *g*-C_3N_4.

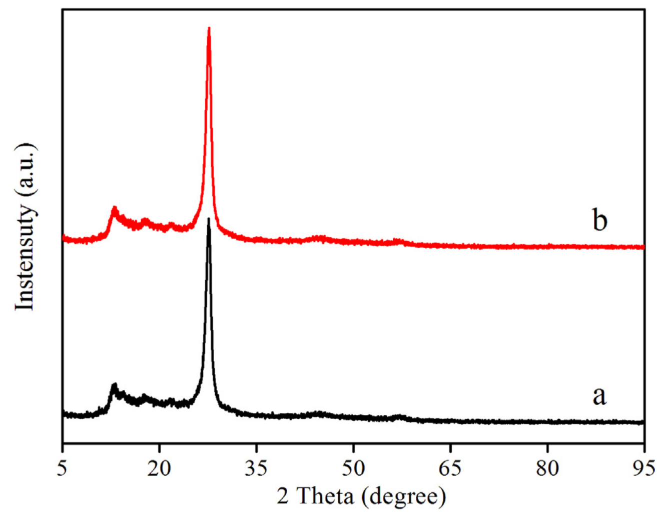

Fig. 1. XRD patterns of pure *g*-C_3N_4 (a) and CPVC/*g*-C_3N_4 (1:300) (b).

XPS analysis was used to determine the chemical states and contents of each element possibly existing on the sample surface. The survey XPS spectra of *g*-C_3N_4 (Fig. 2a) and CPVC/*g*-C_3N_4 (1:300) (Fig. 2b) reveal that the elements of C, O, and N exist on the surface of pure *g*-C_3N_4, while the elements of C, O, N and Cl can be detected in CPVC/*g*-C_3N_4 (1:300) on the basis of the characteristic peaks of 288.1, 529.8, 398.6, and 200.1 eV, which are related to C 1s, O 1s, N 1s and Cl 2p, respectively. The element of Cl comes from CPVC on the surface of *g*-C_3N_4 due to the incomplete removal of chloride atoms from the PVC molecules. This result confirms that the CPVC layer exactly exists on the *g*-C_3N_4 surface.

Fig. 2c and d shows the C 1s XPS spectra of pure *g*-C_3N_4 and CPVC/*g*-C_3N_4 (1:300), respectively, in which the C 1s photoelectron signal has two characteristic peaks at 284.8 and 288.1 eV. The peak at 284.8 eV may be ascribed to the C—C from CPVC on the sample surface or adventitious elemental carbon from the environment. The peak centered at 288.1 eV is attributed to carbon atoms in conjugated structure (—C=C—C=C—) from CPVC and N-containing aromatic rings (—C=N—) which represent the major carbon species in the *g*-C_3N_4 [19,38–40]. Compared with Fig. 2c, the intensity ratio of the two peaks at 288.1 eV and 284.8 eV in Fig. 2d significantly increases, indicating the existence of conjugated structure (—C=C—C=C—) on the surface of CPVC/*g*-C_3N_4 (1:300). This further confirms that CPVC with conjugated structure attaches on the composite surface.

The Raman spectra of pure *g*-C_3N_4 and CPVC/*g*-C_3N_4 (1:300) are shown in Fig. 3. It can be found that the Raman spectrum of CPVC/*g*-C_3N_4 (1:300) (curve b) is very similar to that of *g*-C_3N_4 except for the peak intensity at 1120 cm^{-1} and 1480 cm^{-1}. The characteristic peaks at 1120 cm^{-1} and 1480 cm^{-1} in curve a and curve b are assigned to the C—C and C=C stretching vibrations of the conjugated polymers, respectively [41,42]. The stronger peak intensity at 1120 cm^{-1} and 1480 cm^{-1} in curve b means that CPVC/*g*-C_3N_4 (1:300) possesses more conjugated groups than pure *g*-C_3N_4. The more conjugated groups may be from the conjugated polymer derived from PVC on the *g*-C_3N_4 surface.

The UV–vis diffuse reflectance spectra (UV–vis DRS) of pure *g*-C_3N_4 and the CPVC/*g*-C_3N_4 composites are illustrated in Fig. 4. The absorbance of the CPVC/*g*-C_3N_4 composites is much higher than that of pure *g*-C_3N_4 in the visible light range of 450–800 nm, and increases with the increment of CPVC amount on the composite surface. This indicates that the conjugated polymer obtained from

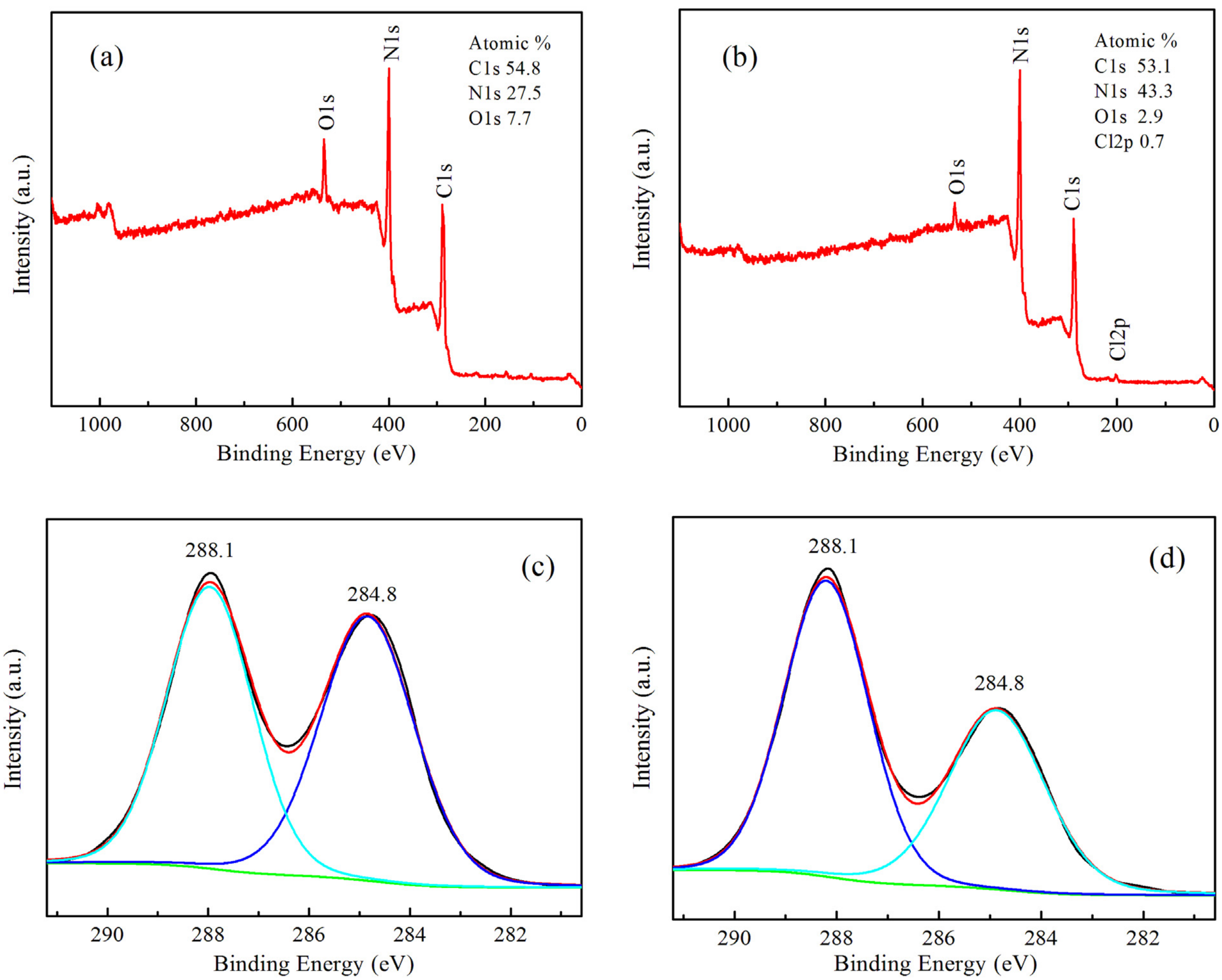

Fig. 2. XPS spectra of g-C_3N_4 and CPVC/g-C_3N_4 (1:300). Survey spectra of g-C_3N_4 (a) and CPVC/g-C_3N_4 (1:300) (b), C 1s of g-C_3N_4 (c) and CPVC/g-C_3N_4 (1:300) (d).

PVC by the heat-treatment at higher temperatures such as 150 °C can be capable of efficiently sensitizing g-C_3N_4, which is favorable to the improvement of the visible-light photocatalytic activity of g-C_3N_4.

The morphology of the materials can be investigated by SEM. Fig. 5 shows the SEM images of pure g-C_3N_4 and CPVC/g-C_3N_4 (1:300). The surface of CPVC/g-C_3N_4 (1:300) is rougher than that of g-C_3N_4 due to the micro-cracks of the composite surface, which is caused by the shrinkage of the CPVC layer during the heat-treatment at 150 °C.

The N_2 adsorption–desorption isotherms of pure g-C_3N_4 and CPVC/g-C_3N_4 (1:300) are shown in Fig. 6. It is easily observed that

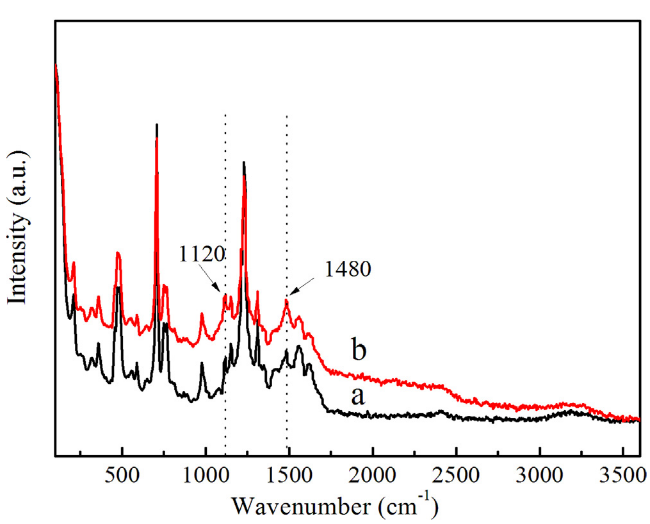

Fig. 3. Raman spectra of pure g-C_3N_4 (a) and CPVC/g-C_3N_4 (1:300) (b).

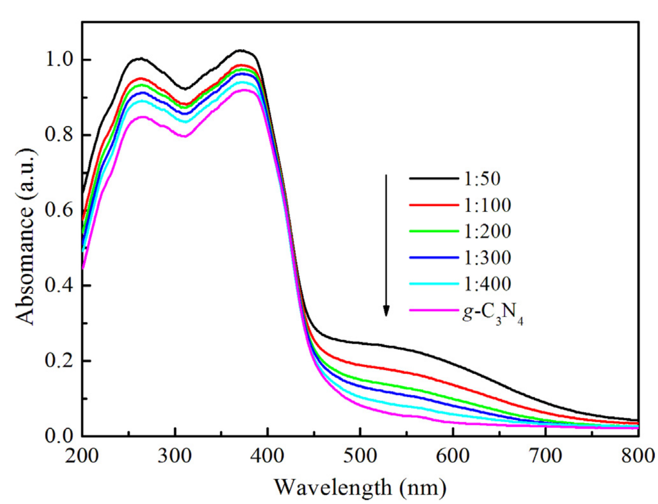

Fig. 4. UV–vis diffuse reflectance spectra of pure g-C_3N_4 and CPVC/g-C_3N_4 composites.

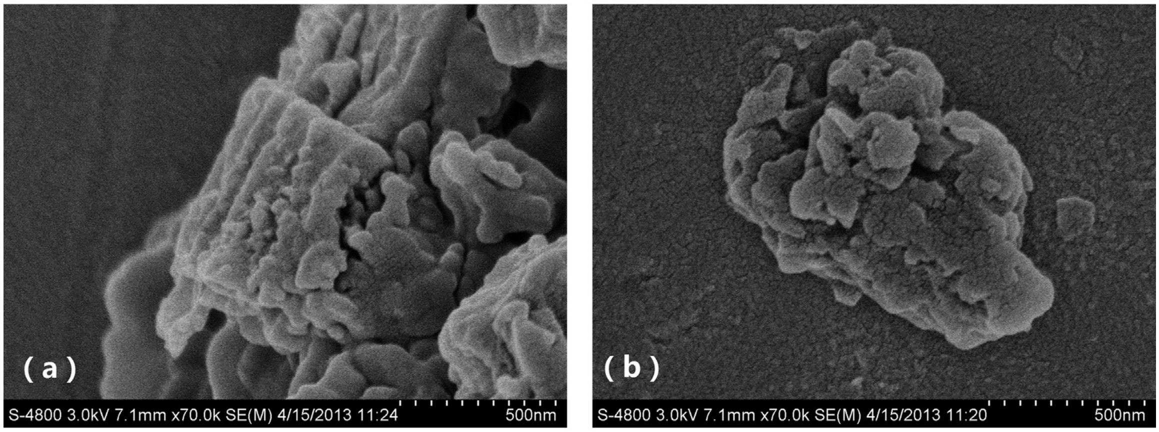

Fig. 5. SEM images of pure g-C_3N_4 (a) and CPVC/g-C_3N_4 (1:300) (b).

both the photocatalysts show type-I isotherm with H3 hysteresis loops. The H3 hysteresis loops might be due to the aggregation of plate-like particles. The BET specific surface area of CPVC/g-C_3N_4 (1:300) is 6.53 $m^2\,g^{-1}$, which is significantly more than that of pure g-C_3N_4 (4.86 $m^2\,g^{-1}$). This result may be caused by the above-mentioned micro-cracks of CPVC layer on the composite surface.

It is well known that PL spectrum is useful to investigate the separation efficiency of the photogenerated electron–hole pairs in semiconductors [43]. The PL spectra of g-C_3N_4 and CPVC/g-C_3N_4 composites are presented in Fig. 7. It can be clearly found that the PL intensity of CPVC/g-C_3N_4 composites is much lower than that of g-C_3N_4, indicating the decrement in the recombination probability between photogenerated electrons and holes, and the increment in the separation efficiency of photogenerated electron–hole pairs. The efficient separation of photogenerated electron–hole pairs in CPVC/g-C_3N_4 composites is probably attributed to the easy transfer of carriers between CPVC and g-C_3N_4.

The EIS technique is widely used to investigate the charge transfer at semiconductor/electrolyte interface [44,45]. The arc radius on EIS Nynquist plots of FTO/CPVC/g-C_3N_4 (1:300) electrode is significantly smaller than that of the FTO/g-C_3N_4 electrode (Fig. 8), revealing that the charge separation efficiency for CPVC/g-C_3N_4 (1:300) is much higher than that for pure g-C_3N_4. This result is in accordance with that of PL spectra.

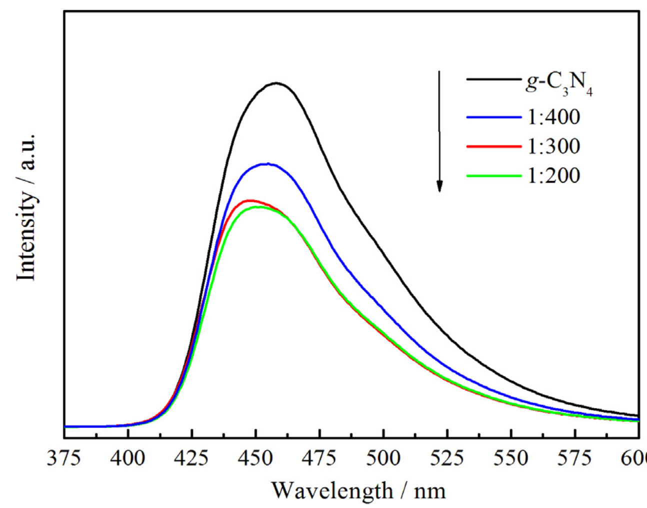

Fig. 7. PL spectra of pure g-C_3N_4 and CPVC/g-C_3N_4 composites.

3.2. *Visible-light photocatalytic activity of CPVC/g-C_3N_4 composites*

The photodegradation rates of RhB under visible-light irradiation without the photocatalyst or in the presence of photocatalyst

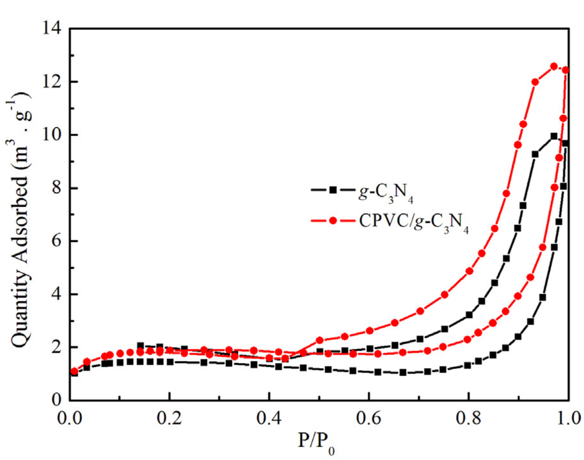

Fig. 6. N_2 adsorption–desorption isotherms of pure g-C_3N_4 and CPVC/g-C_3N_4 (1:300).

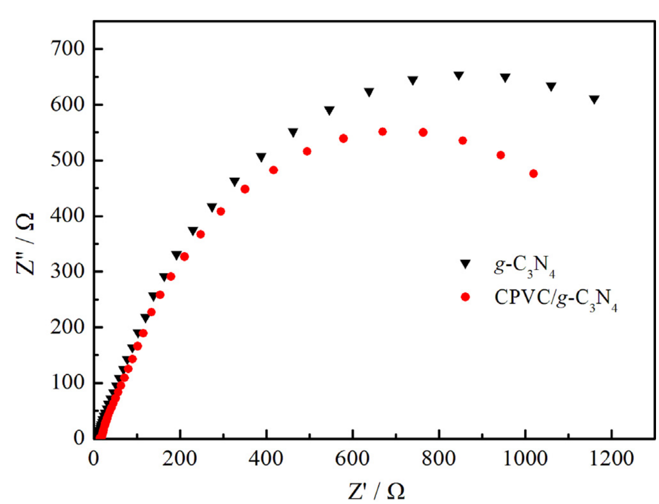

Fig. 8. EIS of FTO/g-C_3N_4 and FTO/CPVC/g-C_3N_4(1:300) electrodes with an applied bias potential of 0.5 V.

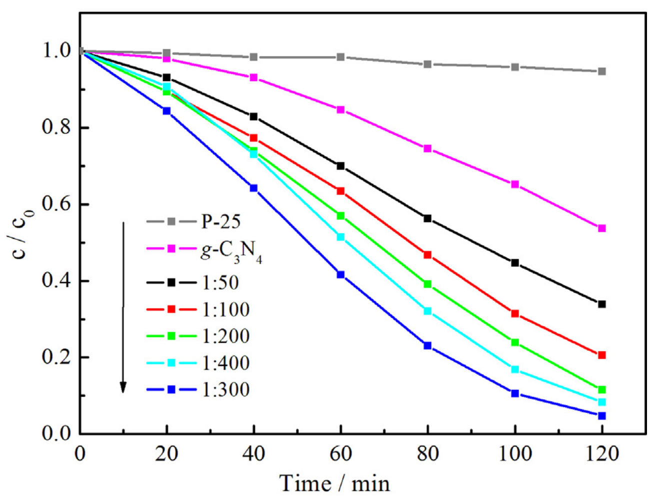

Fig. 9. The relationships between c/c_0 and photodegradation time in the presence of TiO_2 P25, pure g-C_3N_4 and CPVC/g-C_3N_4 composites under visible-light irradiation.

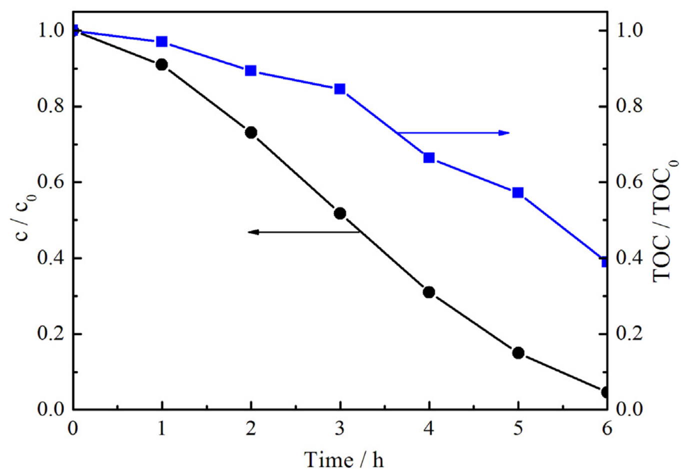

Fig. 11. Decolorization and TOC removal of RhB solution (10 mg L^{-1}, 100 mL) in the presence of CPVC/g-C_3N_4 (1:300) (1 g L^{-1}) under visible-light irradiation.

without visible-light irradiation can be neglected. Figs. 9 and 10 show the relationships between c/c_0 or c_0–c and photodegradation time in the presence of commercial TiO_2 P25, pure g-C_3N_4 and CPVC/g-C_3N_4 composites with different CPVC contents under visible-light irradiation, respectively. It can be found that the RhB degradation under visible-light irradiation in the presence of TiO_2 P25 can be ignored, revealing that the sensitization of RhB is very weak. The RhB photodegradation in the presence of pure g-C_3N_4 and CPVC/g-C_3N_4 composites displays the apparent zero-order kinetic reaction, and the visible-light photocatalytic activities of CPVC/g-C_3N_4 composites are greatly higher than that of pure g-C_3N_4. As the content of CPVC on the composite surface increases, the visible-light photocatalytic activity of CPVC/g-C_3N_4 composites increases at first and then decreases. The CPVC/g-C_3N_4 (1:300) shows the highest visible-light photocatalytic activity, and its apparent rate constant of RhB degradation (0.0277 mg L^{-1} min^{-1}) is over 2.7 times of that of pure g-C_3N_4 (0.0109 mg L^{-1} min^{-1}).

To further confirm RhB degradation photocatalyzed by CPVC/g-C_3N_4 (1:300) under visible-light irradiation, we have carried out TOC measurement and the result is shown in Fig. 11. The RhB solution (10 mg L^{-1}) was nearly decolorized after 6 h under visible-light irradiation and about 60% decrease of TOC has been observed, indicating that RhB has been not only decolorized but also mineralized efficiently.

Besides the photocatalytic activity, the photocatalytic stability is another important factor for a photocatalyst. Fig. 12 reveals that the degradation degree of RhB decreases little with the recycling runs increasing, and is still 90% of that of the first cycling run after 6 recycling runs, indicating that CPVC/g-C_3N_4 (1:300) composite photocatalyst possesses excellent visible-light photocatalytic stability.

3.3. Carriers trapping experiments

The effects of dimethylsulfoxide (DMSO, a typical electron scavenger [46]) and ethylene diamine tetraacetic acid (EDTA, a typical hole scavenger [47]) on the photodegradation rate of RhB in the presence of CPVC/g-C_3N_4 (1:300) were investigated, and the results are shown in Fig. 13. It can be clearly seen that the electron scavenger DMSO slightly decreases the photodegradation rate of RhB, indicating that the photogenerated electrons are not the main active species for RhB degradation. However, the hole scavenger obviously suppresses the RhB photodegradation, revealing that the photogenerated holes are the main active species for RhB degradation.

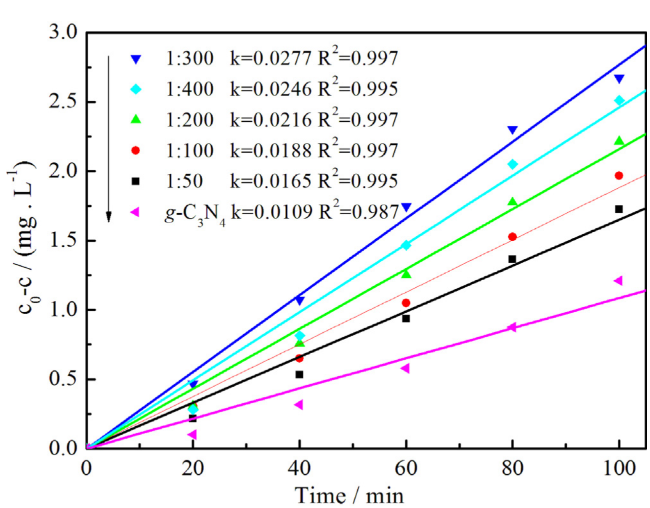

Fig. 10. The relationships between c_0c and photodegradation time in the presence of pure g-C_3N_4 and CPVC/g-C_3N_4 composites under visible-light irradiation.

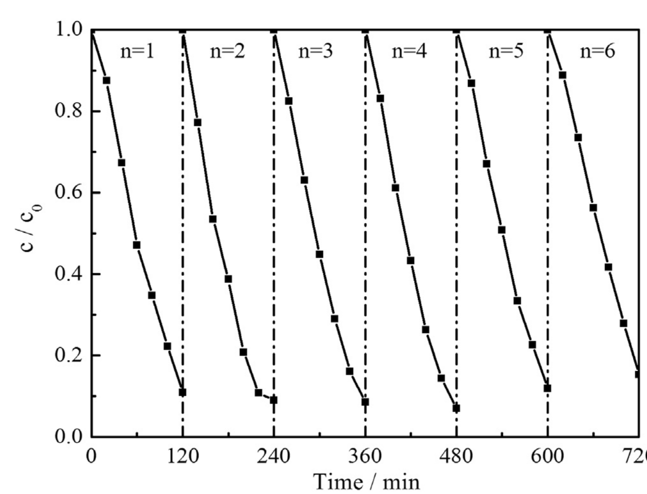

Fig. 12. Cycling runs in photocatalytic degradation of RhB in the presence of CPVC/g-C_3N_4 (1:300) under visible-light irradiation.

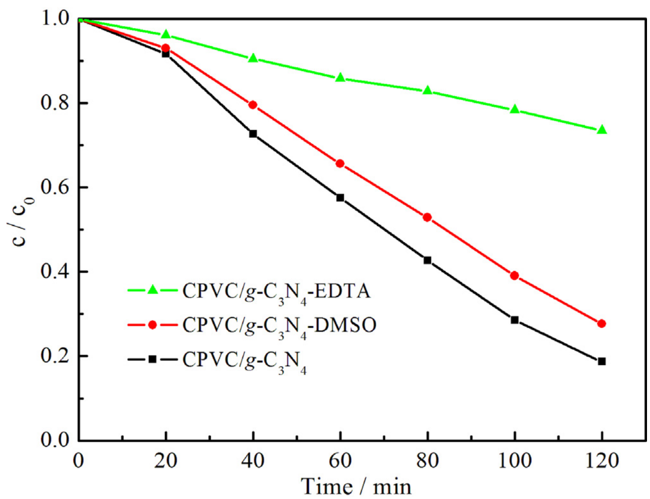

Fig. 13. Effects of DMSO and EDTA on RhB photodegradation catalyzed by CPVC/g-C_3N_4 (1:300) under visible-light irradiation.

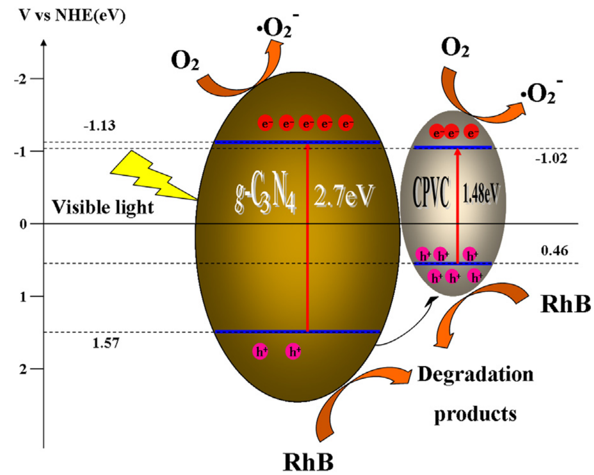

Scheme 3. Schematic description of photocatalytic mechanism of CPVC/g-C_3N_4 photocatalysts under visible-light irradiation.

3.4. *Photocatalytic mechanism of CPVC/g-C_3N_4 photocatalyst*

The HOMO−LUMO gap of CPVC was determined to be ca. 1.48 eV on the basis of the UV−vis diffuse reflectance spectrum (Fig. 14a) [48,49]. The HOMO potential of CPVC can be obtained from the oxidation potential (Eox) in the cyclic voltammetry curve [50,51] as shown in Fig. 14b and is ca. +0.24 V vs. Ag/AgCl electrode, e.g. +0.46 V vs. NHE. Therefore, the LUMO potential of CPVC is ca. −1.02 V vs. NHE. It is widely accepted that the potentials of the valence band (VB) and conduction band (VB) of *g*-C_3N_4 are −1.13 V and +1.57 V vs. NHE, respectively. On the basis of these data, the photogenerated holes in VB of *g*-C_3N_4 are easily be transferred to HOMO of CPVC, however, the photogenerated electrons in CB of *g*-C_3N_4 are difficultly injected into LUMO of CPVC because of little potential difference between CB of *g*-C_3N_4 (−1.13 V) and LUMO of CPVC (−1.02 V). The possible photocatalytic mechanism of the CPVC/*g*-C_3N_4 composites under visible-light irradiation can be schematically presented in Scheme 3.

When the as-prepared composites are irradiated under visible light, both *g*-C_3N_4 and CPVC can easily absorb visible light and be excited to produce photogenerated electron–hole pairs. The photogenerated holes in VB of *g*-C_3N_4 can directly oxidize RhB [16,32]. The photogenerated electrons in CB of *g*-C_3N_4 and LUMO of CPVC can be captured by oxygen adsorbed on the surface of nanocomposite to generate $\bullet O_2^-$ and other active species. The holes, $\bullet O_2^-$, and other active species can be thought to be responsible for the degradation of organic compounds. Due to the obvious potential difference between VB of *g*-C_3N_4 (+1.57 V) and HOMO of CPVC (+0.46 V), the photogenerated holes in VB of *g*-C_3N_4 can be easily transferred to HOMO of CPVC, leading to efficient separation of the photogenerated electron/hole pairs in *g*-C_3N_4. Consequently, the more electrons and holes would exist in the composites, which is favorable to the improvement in the visible-light photocatalytic activity of the investigated composite photocatalysts. The major reactions can be displayed as follows:

$$\mathrm{CPVC}/g\text{-}\mathrm{C_3N_4} + \mathrm{hv} \rightarrow \mathrm{CPVC}*/g\text{-}\mathrm{C_3N_4}*$$

$$\mathrm{CPVC}*/g\text{-}\mathrm{C_3N_4}* \rightarrow \mathrm{CPVC}(\mathrm{e}^-/\mathrm{h}^+)/g\text{-}\mathrm{C_3N_4}(\mathrm{e}^-/\mathrm{h}^+)$$

$$\mathrm{CPVC}(\mathrm{e}^-/\mathrm{h}^+)/g\text{-}\mathrm{C_3N_4}(\mathrm{e}^-/\mathrm{h}^+) \rightarrow \mathrm{CPVC}(\mathrm{e}^-/\mathrm{h}^+\mathrm{h}^+)/g\text{-}\mathrm{C_3N_4}(\mathrm{e}^-)$$

$$\mathrm{h}^+(g\text{-}\mathrm{C_3N_4}) + \mathrm{RhB} \rightarrow \text{Degradation products}$$

$$\mathrm{e}^- + \mathrm{O_2} \rightarrow \bullet\mathrm{O_2}^-$$

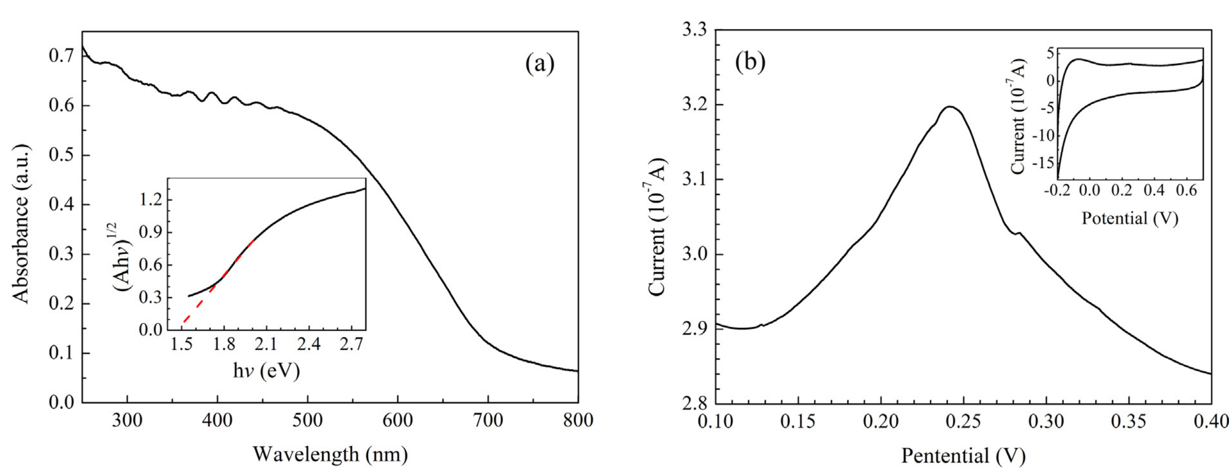

Fig. 14. UV–vis diffuse reflectance spectra of pure *g*-C_3N_4 and its curve of $(Ah\nu)^{1/2}$–$(h\nu)$ (a) and cyclic voltammogram of CPVC film deposited onto ITO glass in 0.1 M $(NH_4)_2SO_4$ solution at a scan rate of 10 mV s^{-1} (b).

$$\bullet O_2^- + 2H^+ + 2e^- \rightarrow \bullet OH + OH^-$$

$$\bullet OH + RhB \rightarrow \text{Degradation products}$$

As the content of CPVC on the composites surface increases, the ability of hole transfer from VB of g-C_3N_4 to CPVC will increase, which can further improve the efficient separation of the photogenerated electron/hole pairs in g-C_3N_4. The more photogenerated holes and electrons benefit the visible-light photocatalytic activity of the CPVC/g-C_3N_4 composite photocatalyst. Nevertheless, when the amount of conjugated polymer on the surface of CPVC/g-C_3N_4 composites is more than a value, the visible light absorbancy of g-C_3N_4 will decrease due to the existence of CPVC layer on g-C_3N_4 surface, leading to the formation of a smaller amount of photogenerated holes and electrons. Additionally, the CPVC layer on g-C_3N_4 surface can decrease the reaction probability between the holes in VB of g-C_3N_4 and RhB in the reaction system. As a result, the visible-light photocatalytic activity of CPVC/g-C_3N_4 composite photocatalysts increases at first and then decreases with increasing the content of conjugated polymer.

4. Conclusions

A new visible-light photocatalyst has been prepared by compounding g-C_3N_4 particles and the conjugated polymer derived from PVC via thermal treatment at 150 °C for 2 h. The spectra of XPS and Raman show that the conjugated polymer derived from PVC exactly exists on the surface of g-C_3N_4. The results of SEM, XRD, BET and UV–vis DRS show that the conjugated polymer can obviously improve the absorbance of g-C_3N_4 particles in the visible light range and their specific surface area, and hardly affect their crystalinity. The visible-light photocatalytic activity of CPVC/g-C_3N_4 composites is much higher than that of the pure g-C_3N_4, and their photocatalytic stability is good. As the CPVC content increases, the visible-light photocatalytic activity increases at first and then decreases, and CPVC/g-C_3N_4 (1:300) possesses the highest visible-light photocatalytic activity. The enhanced photocatalytic activity may be caused by the efficient separation of the photogenerated electron/hole pairs in the as-prepared composites due to the good hole-conductivity of CPVC. Therefore, it is a facile method to prepare a visible-light photocatalyst by the modification of the g-C_3N_4 with a small amount of the conjugated polymer derived from ordinary PVC.

Acknowledgement

This work was supported by Chinese National Science Foundation (No. 21271061) and Hebei Province Science Foundation (No. B2010000846 and B2011208006).

References

[1] A. Fujishima, K. Honda, Nature 37 (1972) 238–250.
[2] Z. Yi, J. Ye, N. Kikugawa, T. Kako, S. Ouyang, H. Stuart-Williams, H. Yang, J. Cao, W. Luo, Z. Li, Y. Liu, R.L. Withers, Nat. Mater. 9 (2010) 559–564.
[3] P. Wang, B. Huang, X. Qin, X. Zhang, Y. Dai, J. Wei, M.H. Whangbo, Angew. Chem. Int. Ed. 47 (2008) 7931–7933.
[4] M. Muruganandham, M. Swaminathan, J. Hazard. Mater. 135 (2006) 78–86.
[5] D. Wang, X. Li, J. Chen, X. Tao, Chem. Eng. J. 198–199 (2012) 547–554.
[6] X. Li, D. Wang, G. Cheng, Q. Luo, J. An, Y. Wang, Appl. Catal. B: Environ. 81 (2008) 267–273.
[7] D. Yang, S.E. Park, J.K. Lee, S.W. Lee, J. Cryst. Growth 311 (2009) 508–511.
[8] J. Choi, H. Park, M.R. Hoffmann, J. Phys. Chem. C 114 (2010) 783–792.
[9] R. Asahi, T. Morikawa, T. Ohwaki, K. Aoki, Y. Taga, Science 293 (2001) 269–271.
[10] D. Chatterjee, A. Mahata, Appl. Catal. B: Environ. 33 (2001) 119–125.
[11] D. Wang, Y. Duan, Q. Luo, X. Li, J. An, L. Bao, L. Shi, J. Mater. Chem. 22 (2012) 4847–4854.
[12] Q. Luo, X. Li, X.Y. Li, D. Wang, J. An, Catal. Commun. 26 (2012) 239–243.
[13] M.L. Tang, D.C. Grauer, B. Lassalle-Kaiser, V.K. Yachandra, L. Amirav, J.R. Long, J. Yano, A.P. Alivisatos, Angew. Chem. Int. Ed. 50 (2011) 10203–10207.
[14] Y. Bi, S. Ouyang, N. Umezawa, J. Cao, J. Ye, J. Am. Chem. Soc. 133 (2011) 6490–6492.
[15] D. Wang, Y. Duan, Q. Luo, X. Li, L. Bao, Desalination 270 (2011) 174–180.
[16] X.C. Wang, K. Maeda, A. Thomas, K. Takanabe, G. Xin, J.M. Carlsson, K. Domen, M. Antonietti, Nat. Mater. 8 (2009) 76–80.
[17] H. Pan, Y.W. Zhang, V.B. Shenoy, H. Gao, ACS Catal. 1 (2011) 99–104.
[18] A. Du, S. Sanvito, Z. Li, D. Wang, Y. Jiao, T. Liao, Q. Sun, Z. Zhu, R. Amal, S.C. Smith, J. Am. Chem. Soc. 134 (2012) 4393–4397.
[19] S.W. Cao, Y.P. Yuan, J. Fang, M.M. Shahjamali, F.Y.C. Boey, J. Barber, S.C.J. Loo, C. Xue, Int. J. Hydrogen Energy 38 (2013) 1258–1266.
[20] J.A. Singh, S.H. Overbury, N.J. Dudney, M. Li, G.M. Veith, ACS Catal. 2 (2012) 1138–1146.
[21] F. Wu, Y. Liu, G. Yu, D. Shen, Y. Wang, E. Kan, J. Phys. Chem. Lett. 3 (2012) 3330–3334.
[22] Q. Xiang, J. Yu, M. Jaroniec, J. Phys. Chem. C 115 (2011) 7355–7363.
[23] G. Dong, K. Zhao, L. Zhang, Chem. Commun. 48 (2012) 6178–6180.
[24] Y. Wang, X. Bai, C. Pan, J. He, Y. Zhu, J. Mater. Chem. 22 (2012) 11568–11573.
[25] G. Liao, S. Chen, X. Quan, H. Yu, H. Zhao, J. Mater. Chem. 22 (2012) 2721–2726.
[26] J. Zhang, J. Sun, K. Maeda, K. Domen, P. Liu, M. Antonietti, X. Fu, X. Wang, Energy Environ. Sci. 4 (2011) 675–678.
[27] J. Hong, X. Xia, Y. Wang, R. Xu, J. Mater. Chem. 22 (2012) 15006–15012.
[28] X.F. Chen, J.S. Zhang, X.Z. Fu, M. Antonietti, X. Wang, J. Am. Chem. Soc. 131 (2009) 11658–11659.
[29] Y. Zhang, T. Mori, J. Ye, M. Antonietti, J. Am. Chem. Soc. 132 (2010) 6294–6295.
[30] L. Zhang, X. Chen, J. Guan, Y. Jiang, T. Hou, X. Mu, Mater. Res. Bull. 48 (2013) 3485–3491.
[31] L. Sun, X. Zhao, C. Jia, Y. Zhou, X. Cheng, P. Li, L. Liu, W. Fan, J. Mater. Chem. 22 (2012) 23428–23438.
[32] L. Ge, C.C. Han, J. Liu, J. Mater. Chem. 22 (2012) 11843–11850.
[33] E.D. Owen, M. Shah, N.J. Everall, M.V. Twigg, Macromolecules 27 (1994) 3436–3438.
[34] M. Rogestedt, T. Hjertberg, Macromolecules 26 (1993) 60–64.
[35] E.W. Michell, J. Mater. Sci. 20 (1985) 3816–3830.
[36] W.H. Starnes, X. Ge, Macromolecules 37 (2004) 352–359.
[37] P. Niu, G. Liu, H.M. Cheng, J. Phys. Chem. C 116 (2012) 11013–11018.
[38] L. Ge, C. Han, J. Liu, Y. Li, Appl. Catal. A: Gen. 409–410 (2011) 215–222.
[39] Y. Wang, X. Wang, M. Antonietti, Angew. Chem. Int. Ed. 51 (2012) 68–89.
[40] A. Vinu, Adv. Funct. Mater. 18 (2008) 816–827.
[41] S. Ellahi, R.E. Hester, K.P.J. Williams, Spectrochim. Acta A 51 (1995) 549–553.
[42] D.L. Gerrard, W.F. Maddams, Macromolecules 8 (1975) 54–58.
[43] F. Tian, Y. Zhang, J. Zhang, C. Pan, J. Phys. Chem. C 116 (2012) 7515–7519.
[44] W.H. Leng, Z. Zhang, J.Q. Zhang, C.N. Cao, J. Phys. Chem. B 109 (2005) 15008–15023.
[45] Y. Duan, Q. Luo, D. Wang, X. Li, J. An, Q. Liu, Superlattice Microstruct. 67 (2014) 61–71.
[46] Y. Zhao, C. Eley, J. Hu, J.S. Foord, L. Ye, H. He, S.C.E. Tsang, Angew. Chem. Int. Ed. 51 (2012) 3846–3849.
[47] N. Serpone, I. Texier, A.V. Emeline, P. Pichat, H. Hidaka, J. Zhao, J. Photochem. Photobiol. A 136 (2000) 145–155.
[48] B. Wang, H.A. Xi, J. Yin, X.F. Qian, Z.K. Zhu, Synth. Met. 139 (2003) 187–190.
[49] F. Yakuphanoglu, M. Arslan, Solid State Commun. 132 (2004) 229–234.
[50] S.C. Price, A.C. Stuart, L. Yang, H. Zhou, W. You, J. Am. Chem. Soc. 133 (2011) 4625–4631.
[51] Q. Luo, L. Bao, D. Wang, X. Li, J. An, J. Phys. Chem. C 116 (2012) 25806–25815.